In situ AFM study of near-surface crystallization in PET and PEN

Kei Shinotsuka, Hazel Assender

Department of Materials, University of Oxford, Parks Road, Oxford OX1 3PH, United Kingdom
Correspondence to: H. Assender (E-mail: hazel.assender@materials.ox.ac.uk)

ABSTRACT: The surface crystallization behavior of poly(ethylene terephthalate) (PET) and poly(ethylene 2,6-naphthalate) (PEN) spin-coated thin films was compared by means of atomic force microscopy (AFM) with an *in situ* heating stage. As the films were heated up stepwise, characteristic surface crystals appeared at a crystallization temperature (T_c) in the near-surface region which is about 15 °C under the bulk T_c, and were replaced by bulk crystals when the temperature was increased to the bulk T_c. In the case of films whose thickness is less than 70 nm (PET) and 60 nm (PEN), significant increases in the bulk T_c were observed. Scanning force microscopy (SFM) force-distance curve measurements showed that the glass transition temperature (T_g) of the near-surface region of PET and PEN were 22.0 and 26.6 °C below their bulk T_g (obtained by DSC). After the onset of surface crystallization, edge-on and flat-on crystals appeared at the free surface of PET and PEN thin films, whose morphologies are very different to those of the bulk crystals. Although the same general behavior was observed for both polyesters, there are significant differences both the influence of the surface and substrate on the transition temperatures, and in morphology of the surface crystals. These phenomena are discussed in terms of the differences in the mobility of polymer chains near the surface. © 2016 Wiley Periodicals, Inc. J. Appl. Polym. Sci. **2016**, *133*, 44269.

INTRODUCTION

Comprehensive understanding of the properties of the polymer surface and polymer thin films has become more important recently, in many applications such as multi-layer films, coatings, adhesives, thin layer electronic devices (organic light emitting diodes and organic photovoltaic cells), optoelectronics, and so on.

Typical polymeric crystallization processes have been fully studied using films of a few micrometers in thickness.[1–3] In the case of very thin polymer films, whose thickness is less than, for example, 100 nm, however, the influence of the surface and any underlying interface increases, so that the effect of interfacial polymer chain behavior can become the dominating feature of polymer crystallization. Various studies have been carried out for nanometer thick films, and unique thin-film crystals have been reported for several different polymers such as polystyrene,[4–6] polylactide,[7–9] poly(ethylene oxide),[10–12] and poly(ethylene terephthalate).[13,14] In this thickness range, single lamellar crystals such as flat-on and edge-on lamellar crystals are produced, whereas as the thickness becomes smaller, self-diffusion is restricted due to the confinement of the chains within the thin layer, and a non-equilibrium crystalline morphology such as seaweed or finger pattern appears reflecting the inhomogeneity of the self-diffusion at the growth front caused by local thermodynamic fluctuations. However, these studies have considered the crystallization processes during which the molecules in the whole polymer film have been mobile, and crystallization studies specific to the near-surface region have not been significantly reported.

The understanding of the surface crystallization of thin films is closely linked with the study of glass transition behavior, as the T_g is known to be modified at the near-surface. It is well-established that the polymer near an interface can show a modified T_g, with many studies reporting a decreased T_g near the free-surface, leading to an overall decrease in T_g of a thin film, within which the surface has a significant influence.[15–25] Our group[26] has also observed T_g depression by several °C in polystyrene (PS) films on a silicon substrate, by means of SFM force distance curve measurements.

Cold crystallization from glassy amorphous material begins when a film is heated up above the observed T_c, which is some temperature above T_g; previously we have reported[27] how the low T_g near the PET free surface can be exploited to produce surface-specific crystallization by annealing at temperatures between the surface T_c and the bulk T_c.

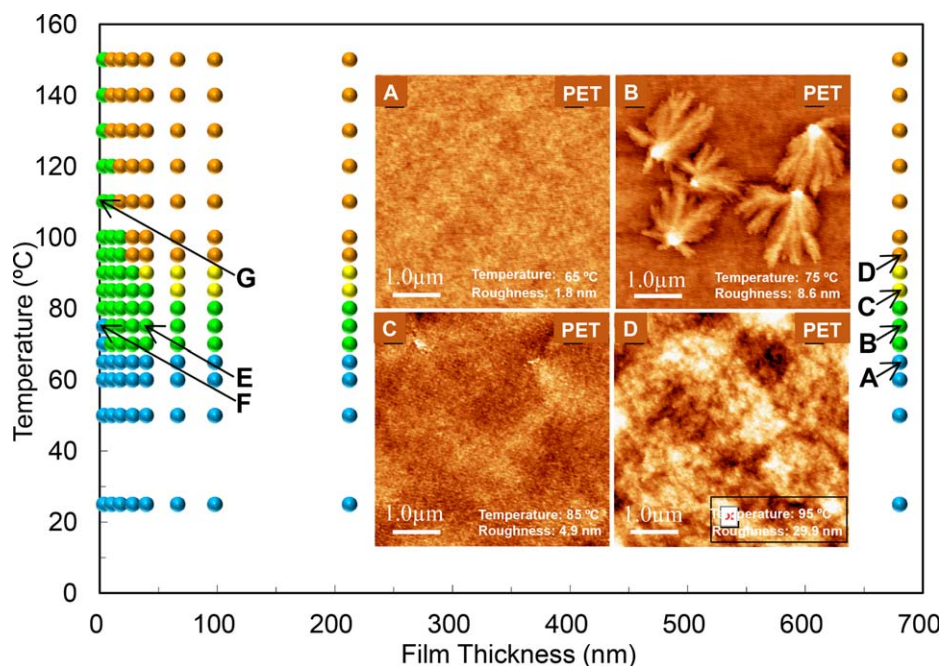Additional Supporting Information may be found in the online version of this article.

Figure 1. Surface morphology of PET thin films after a 2 h anneal at each temperature in increasing steps. From low T to high T: Blue: amorphous, Green: surface crystals, Orange: bulk crystallinity. Yellow (between green and orange) represents an intermediate structure in which the surface crystalline morphology has not yet been fully broken up by the onset of bulk crystallization. Insets are AFM images of representative morphologies of each colored region. [Color figure can be viewed at wileyonlinelibrary.com.]

In this study, we compare the surface crystallization behavior of PET and PEN spin coated thin films, observing the influence of film thickness and annealing temperature, to consider the influence of the relatively rigid molecular structure and higher T_g of PEN on the surface crystallization behavior, and we make a careful comparative analysis of the surface crystalline morphology for both polymers.

EXPERIMENTAL

Materials
PET pellets (density = 1.375 g/cm³) were purchased from Sigma Aldrich. PEN pellets (density = 1.33 g/cm³) were kindly provided from Teijin Chemical Co., Ltd. Their viscosity average molecular weights were measured to be 26000 g/mol and 15000 g/mol, respectively.

PET and PEN were each fully melted and crash cooled before being dissolved in a mixed solvent of 70 wt % 2-chlorophenol (Fisher Scientific) and 30 wt % 1,1,1,3,3,3-hexafluoro-2-propanol (Sigma Aldrich) at 100 °C with ultrasound. Solutions were filtrated with 0.2 µm pore sized PTFE filters.

Amorphous polymer films were formed on single crystal silicon substrates (orientation (100)) by spin coating at 3000 rpm to give the very low roughness films associated with the amorphous structure.[27] After deposition, the films were dried under vacuum for more than 6 h. Film thicknesses were controlled in the range from 3 nm to 700 nm, measured by an ellipsometer (Rudolph Research/Auto EL) and AFM.

In Situ AFM Observation and Force-Distance Curve
Each sample cast on a Si substrate was set on a specially designed in situ heating stage placed on an AFM scanner, and

annealed at elevated temperatures ranging from 50 to 150 °C for PET and from 70 to 190 °C for PEN. The heating was performed stepwise and samples were kept at each increasingly elevated temperature for 2 h before the morphology was recorded.

The morphology change of the films during the crystallization process has been observed depending on film thickness and temperature of crystallization. An auto-probe CP microscope (Park Scientific Instruments) with V-shaped cantilever (Thermo microscopes "Ultralever," effective nominal tip radius of 10 nm, spring constant ranging from 1.1 to 1.6 N/m) was operated in contact mode for AFM topography and lateral force microscopy (LFM) images. The scanning was performed at a rate of 0.5–0.7 Hz.

Measurement of the surface T_g can give a better understanding of the surface crystallization phenomenon. In this study, SFM force-distance curve measurement was used to determine the surface T_g of PET and PEN films, which can detect the slight change in elasticity on the surface,[26,27] by means of the same in situ heating stage with the V-shaped cantilever, at a contact force of 0.24 nN and a scanning rate of 0.7 Hz.

DSC
The bulk T_g of PET and PEN as-received pellets were measured by differential scanning calorimetry (Perkin Elmer DSC-7) at a heating rate of 5 °C/min in an argon gas atmosphere.

RESULTS AND DISCUSSION

PET Surface Crystals and the Crystal Stability Diagram
Figure 1 represents the PET crystal stability diagram which is based on the AFM morphological observation of the surface features after each annealing temperature as a function of film
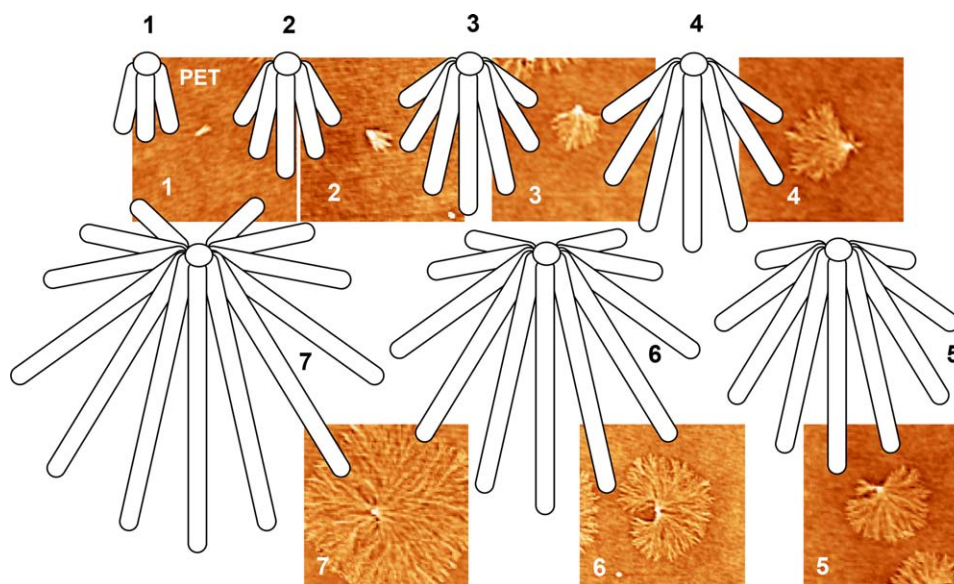
Figure 2. Schematic model of lamellae development of a PET surface crystal with fan-shape morphology. As the surface crystal develops, other new lamellae derive from the core adjacent to the crystal which is already formed. There is increase of angle in developing direction of surface crystals. AFM images are corresponding surface crystals on 39 nm thick PET films. As the angle increases, crystal growth dimension shifts from 1D to 2D. [Color figure can be viewed at wileyonlinelibrary.com.]

thickness. The surface states were categorized as amorphous, surface crystalline, and bulk crystalline. Representative AFM images of each of the characteristic morphologies are shown using an example sequence of temperatures with the 680 nm film. A more detailed discussion of these observations can be found in.[27]

The PET crystal stability diagram shows the characteristic behavior of surface crystallization as follows:

1. The onset of the surface T_c is observed at 70 °C which is 15 °C lower than that of the bulk crystallization (85 °C).
2. There is a dendritic surface crystalline region with a range of about 15 °C in temperature for all thicknesses greater than 70 nm films, irrespective of film thickness.
3. When the film thickness is less than about 70 nm, surface crystals are stable up to a much higher temperature than the bulk T_c of thicker films. For example, bulk crystallization morphology in 10 nm thick film is not observed until 130 °C, which is 45 °C higher than that of thick films. This is presumably due to the influence from the substrate layer, restricting the molecular mobility in the bulk layer near the bottom interface. Thus, as the film thickness decreases, this influence from the substrate layer increases, resulting in the increase of the apparent bulk T_c. An alternative or additional explanation could be the increase in molecular anisotropy resulting from the spin-coating process[28–30] as the film thickness decreases.
4. PET surface crystals show characteristic fan-shape morphology. Figure 2 shows a schematic model of lamellae development of a typical PET fan-shape crystal. As the surface crystal develops, other new lamellae derive from the core adjacent to the crystal which is already formed. There is an increase in the range of angle over which surface crystals

develop, such that crystal growth dimension shifts from one-dimensional (1D) to two-dimensional (2D).

5. The interlamellar wavelength of PET surface crystals at 80 °C for each film thicknesses is shown in Figure 3. The determination of the length from one crystal lamella to the next (the "wavelength") was carried out both by direct measurement from the AFM topography, and by calculation of power spectral density based on Fourier transform. As the film thickness becomes larger, the wavelength increases linearly. The surface waves of films thicker than 210 nm became indistinct, and it was difficult to define the wavelength.
6. The surface crystalline morphology is destroyed after the onset of bulk crystallization at 85 °C by the much rougher bulk crystallization morphology.
7. The very thinnest, 3 nm thick, film showed different surface crystallite morphology. At this thickness, the onset of surface T_c is about 10 °C higher than that of other film thicknesses, and surface crystals were not replaced by bulk crystals even at 150 °C.

PEN Surface Crystals and the Crystal Stability Diagram

The PEN crystal stability diagram based on each processing temperature and film thickness is shown in Figure 4. As in the case of PET, the surface state was categorized as amorphous, surface crystalline, intermediate, and bulk crystalline regions. Figure 5 shows examples of surface morphologies of PEN films; each image corresponds to the labelled points in Figure 4.

The common points between the PET and PEN crystal stability diagrams are as follows:

1. For PEN the surface T_c and the bulk T_c were observed at 115 and 130 °C respectively. Between these temperatures dendritic surface crystals are observed [Figure 5(A1–F1)].
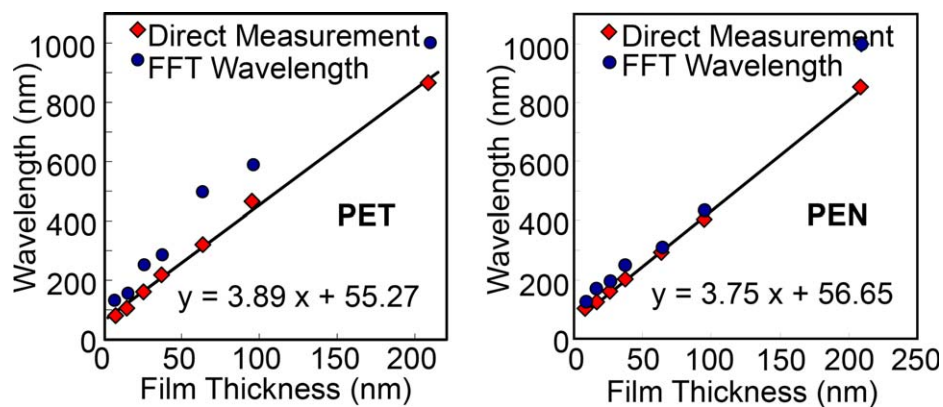
Figure 3. The interlamellar wavelength of the dendritic structure of PET and PEN surface crystals obtained by direct measurement from observed lamellar structures in AFM images (diamonds), and the wavelength values calculated by power spectral density based on Fourier transform of the whole AFM images (circles), as a function of film thickness. The regression lines (applied to the AFM data) indicate that the wavelength is proportional to the film thickness. The crystallization temperature of PET and PEN are 80 and 125 °C, respectively. [Color figure can be viewed at wileyonlinelibrary.com.]

For both polymers there is a surface crystalline region spanning 15 °C in between the amorphous and bulk crystalline regions in thicker films. In thicker films, as the temperature is raised, the surface crystals were swiftly broken down by bulk crystals: for PEN, at 130 °C [e.g., Figure 5(A2), 210 nm thick].

2. As in the case of PET, as the films become thinner, the width of the dendritic branches of PEN surface crystals decreases,[27] shown in Figure 5(A1–F1). The wavelength of PEN surface crystals at 125 °C for each film thickness is shown in Figure 3 to increase linearly with film thickness (The best fit line to the graph for PEN being 3.75x + 56.65 – very similar to that of PET).

3. As the film thickness decreases (below about 60 nm for PEN), the thermal stability of surface crystals greatly improves and the bulk T_c shifts to higher temperature. In the case of film 9 nm or thinner, the surface crystalline

Figure 4. Crystal stability diagram of PEN thin films heated up stepwise and kept at each elevated temperature for 2 h. The surface features are categorized (from low T to high T) as amorphous (Blue), surface crystalline (Green), intermediate structure between surface and bulk crystalline (Yellow), and bulk crystalline (Orange). Labelled points A1-G2 correspond to AFM images shown in Figures 5–7. [Color figure can be viewed at wileyonlinelibrary.com.]

structure is sustained until at least 190 °C which is far higher than the bulk T_c in the thicker films. Image F2 of Figure 5 shows the dendritic structure on a 9 nm thick film still stable at 150 °C, although some amorphous surface is still observed even at 150 °C.

4. The surface T_c of very thin films (9 and 3 nm) is larger than that of other film thicknesses. In particular, the 3 nm thick film starts surface crystallization at 180 °C, indicating significant inhibition of crystallization.

At the same time, there are some dissimilarities:

1. PEN dendritic surface crystals are more finely branched than that of PET. The branching points occur more frequently during the growing process, and the average angle at a junction is larger than that of PET [e.g., compare Figure 9(a) with Figure 5(E1)]. The intersection of the branches form an angle of about 30°–60°. Thus for PEN, branching of the crystals to bring in more local material to the crystal structure is more favored than single direction growth seen in the more mobile PET.

2. As the film thickness increases, there appear many fine bristle-like perpendicular projections on the surface crystals (They are clearest in images A1 and B1 in Figure 5), which are not observed in PET crystals.

3. Even in the case of thin films, PEN surface crystals radiate from every direction from the very beginning of surface crystallization, for example, Figure 5(F1), while PET nascent surface crystals can grow within a limited angle.

4. The surface crystals of PET and PEN protrude by a few nm from the surrounding amorphous surface level. Growth of the surface crystals involves mass depletion at the lamellar growth front, creating an adjacent depression surrounding the surface crystals (Figure 6). The volume of the surface crystal protruding above the surface level approximately corresponds with the volume of the surrounding depression under the surface level. In general, the surface crystals in PEN were found to protrude further from the amorphous surface than those of PET.
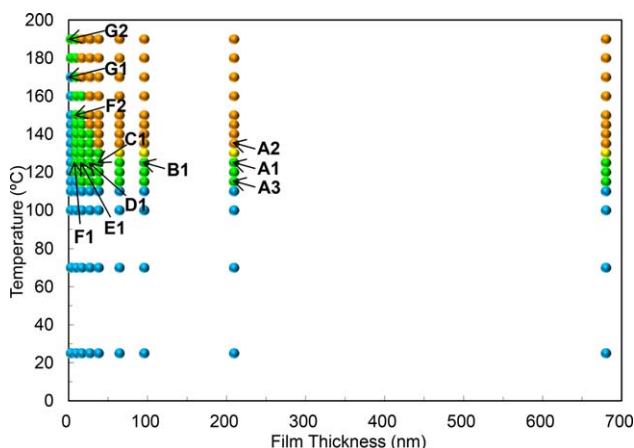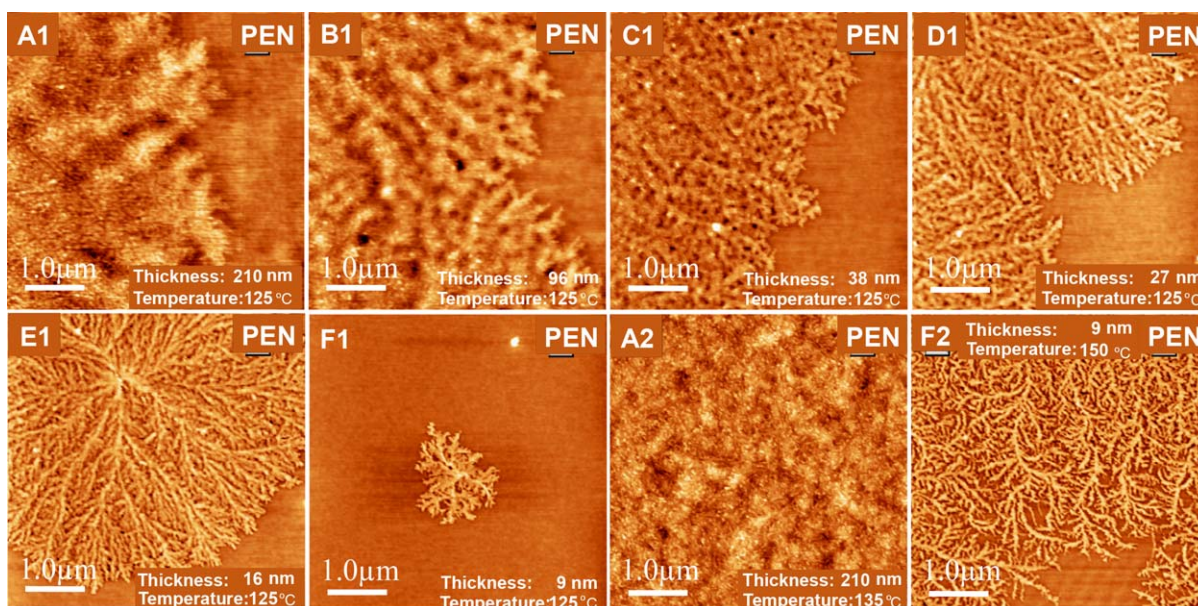
Figure 5. Surface crystals of PEN films at 125 °C are shown from A1 to F1. The wavelength (width) of dendritic surface crystalline branches decreases with decreasing film thickness. As the film thickness becomes larger, there appear many fine bristle-like projections on the surface crystals, which are obvious in A1 and B1. In thick films such as A2, surface crystals were swiftly overtaken by bulk crystals as the temperature is raised to 135 °C. In thinner films, the thermal stability of surface crystals was significantly improved. F2 shows the dendritic surface crystalline structure still withstanding at 150 °C which is higher than the bulk T_g in thicker films. Images A1–F2 correspond to the labelled points in Figure 4. [Color figure can be viewed at wileyonlinelibrary.com.]
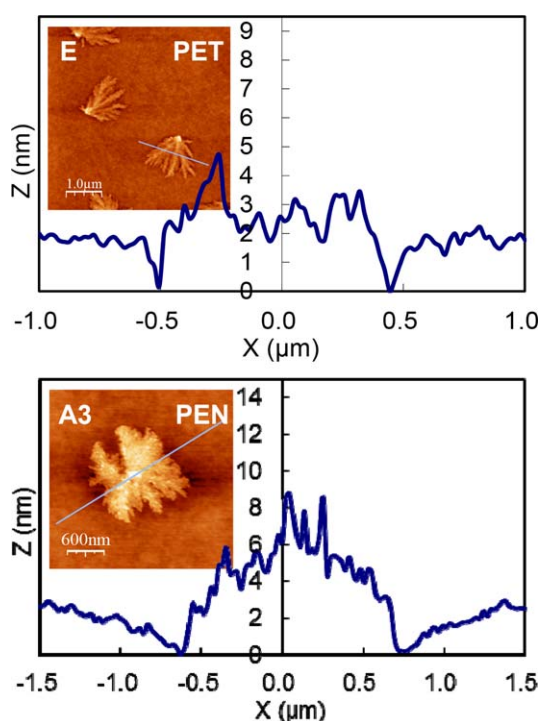

Figure 6. Topographic line profile of PET (39 nm, annealed at 75 °C for 2 h) and PEN (209 nm, annealed at 115 °C for 2 h) surface crystals, surrounded by 2 and 3 nm deep trench. The image corresponds to labelled point E in Figures 1 and A3 in Figure 4 respectively. The cross sections correspond to the straight lines in the image inserted above. [Color figure can be viewed at wileyonlinelibrary.com.]

5. As in PET, the thinnest (3 nm) PEN film exhibits characteristic crystalline morphology which differs from the thicker films. Figure 7(a) shows amorphous flat surface still stable, in this example in PET even at 75 °C (10 °C above the thick film surface crystallization temperature). As annealing temperature increases, the PET and PEN amorphous surface forms many fine dimples [and example for PET is shown in Figure 7(b), showing dimpled region outside the crystals, and example for PEN is shown in Figure 7(c)], possibly due to initial thermal molecular relaxation of polymer molecules which are not completely free from the original position due to the interaction with the substrate. At the onset of surface crystallization (80 and 180 °C for PET and PEN respectively at this thickness) the two polymers show different morphologies. In the 3 nm PET film [Figure 7(b)], crystals grew at the higher points of the dimpled amorphous surface (where more material is available for reorganization), forming a characteristic morphology with peak-to-trough height of around 5.5 nm. At this thickness, there is limited self-diffusion caused by thickness confinement as well as any anchoring effect of the surface molecules which will have direct contact with the substrate surface. Thereby, the molecules cannot be transported for a long distance to the growth front by self-diffusion. It is thought that this limited molecular supply produces the peculiar crystalline morphology in which branched line-shape crystals proliferate seeking "high" places on the dimpled surface. In contrast to PET, PEN can only form crystals in these films at more highly elevated temperatures (65 °C above the thick film surface crystallization temperature). Similar to PET, 3 nm PEN amorphous film develops finely dimpled surface [Figure
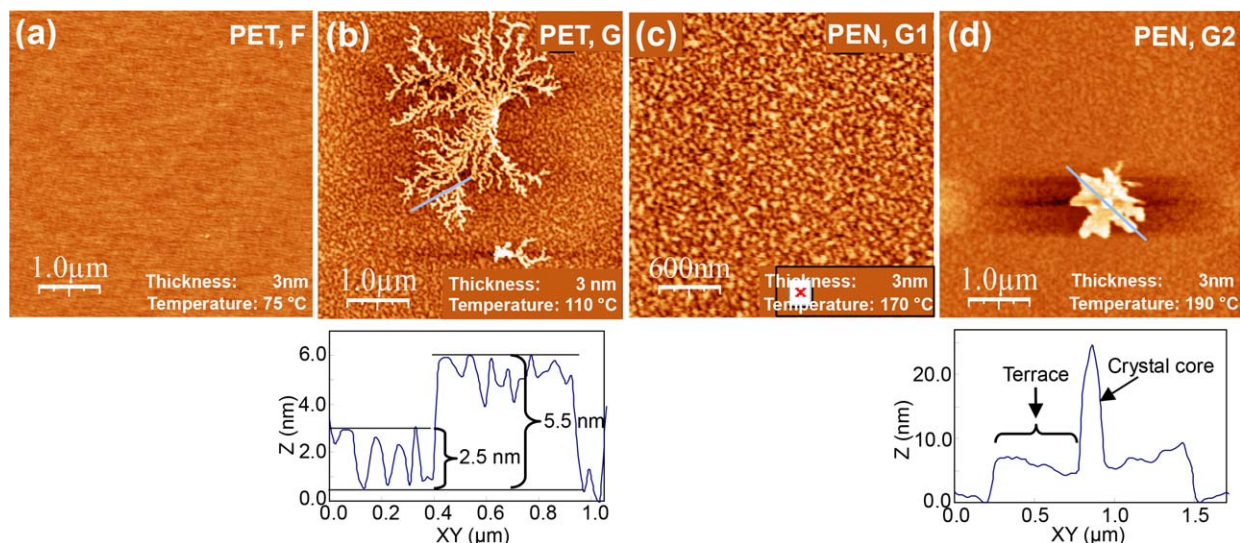
Figure 7. (a) 3 nm PET film after 75 °C-2 h at which, even after annealing at this elevated temperature, does not show crystallization, showing the flat amorphous surface. (b) 3 nm PET film after 110 °C-2 h annealing: the original amorphous surface develops numerous dimples and surface crystals proliferate thorough the "high" points on the surface. The height profile shows that the amplitude of surface dimples and surface crystals are consistently 2.5 and 5.5 nm respectively. (c) 3 nm PEN film after 170 °C-2 h at which, even after annealing at this elevated temperature, does not show crystallization, rather the amorphous surface shows many small dimples. (d) 3 nm PEN film after 190 °C-2 h annealing shows how the original amorphous surface develops numerous dimples and a surface crystal with a protruding core. The height profile shows that the surface terrace-like crystal around this core has a constant thickness of about 7.0 nm. Images (a) and (b) corresponds to the labelled points F and G respectively in Figure 1, and Images (c) and (d) correspond to the labelled points G1 and G2 respectively in Figure 4. [Color figure can be viewed at wileyonlinelibrary.com.]

7(c)] up to just before the onset of crystallization. When PEN does eventually crystallize, it forms highly localized disc-like crystals with thickness of ca. 7.0 nm [Figure 7(d)] around a protruding nucleus. The constant crystal thickness suggests that the lamellar orientation of the PEN crystal is flat-on. In the PEN case, nucleation of a crystal can only be achieved by a very local, very high [25 nm in Figure 7(d)] protrusion from the surface, whereas PET can crystallize more readily wherever there is a slightly thicker layer of material at temperatures only 10 °C above the surface crystallization temperature of thick films.

One clear point is that the dimpled amorphous surface we observed is not created by dewetting of the thin polymer layer against the substrate, but formed by enhanced molecular thermal mobility at the near-surface with the molecules anchored onto the substrate surface. This is because, if the dimples were dewetting, PEN surface crystals would not grow out to such large size because of the discontinuity of polymer material on the substrate.

In the case of these ultra-thin films there is no bulk material available and so the bulk crystal morphology is not observed.

Surface T_g and T_c of PET and PEN
A different molecular mobility at different depths through the thickness of a polymer thin film has been proposed.[31] In this case three "layers," a near-surface region, a bulk region and a near-substrate region were proposed in the case of poly(bisphenol A hexane ether). In addition, there is extensive literature reporting a depressed T_g at the free surface of a polymer, and

also on the effect of an underlying substrate on the T_g of a supported thin film.[15–24] To summarize this literature: at most thicknesses of an amorphous supported film, the surface layer is thought to be a thin layer with T_g lower than that of the bulk layer. The substrate layer is thought to have another intrinsic T_g as well, which is influenced by the interaction with the substrate surface. The bulk layer exists in between the surface and substrate layers.

Based on the observed crystallization behavior we have shown that both PET and PEN follow crystallization processes influenced by the different mobility near the free surface and near the substrate.[27] As the annealing temperature is increased, the surface crystallization starts at the surface T_c which is lower than the bulk T_c by 15 °C. Due to the small thickness of the surface layer, surface crystals grow two dimensionally, exhibiting distinct lamellar morphology. Direct observation of the surface topography, rather than diffractometric investigation, enables the detection of surface crystallization at the lowest temperature.[32]

Above the bulk T_c, the bulk crystallization takes place and the bulk crystallites, with typical spherulitic morphology,[33] break up the surface integrating the 2D surface crystals, and thereafter the dendritic crystalline morphology is totally replaced by bulk crystals.

In the case of ultra-thin films, less than 10 nm thick, there is no longer a thickness of "bulk layer," so that the surface layer and the substrate layer impinge on each other. In this special case, the bulk crystallization onset is not observed, and an increase of surface crystallization temperature is observed. This agrees with recent simulation data that structural relaxation is
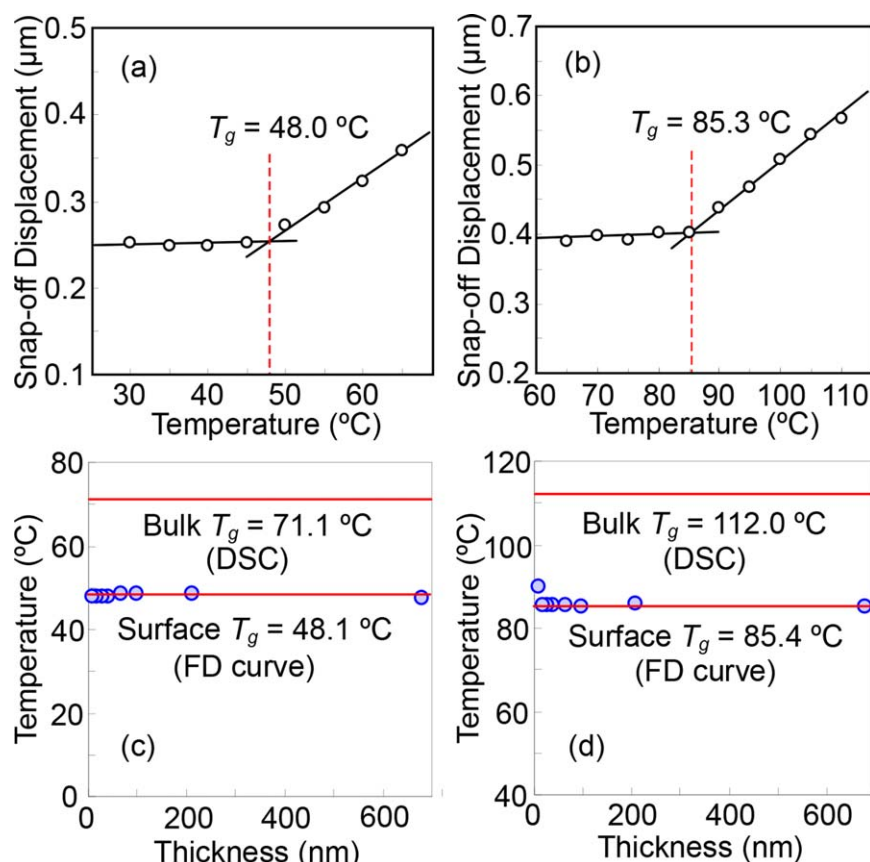
Figure 8. (a) Surface T_g determination of PET 27.6 nm thick film by means of the change of snap-off displacement in the SFM force-distance curve. The plot indicates surface elasticity changes at 48.0 °C. (b) Surface T_g determination of PEN 26.6 nm thick film by means of the change of snap-off displacement in the SFM force-distance curve. The plot indicates surface elasticity changes at 85.3 °C. (c) Surface T_g obtained by force-distance curve for PET films of each thickness. A constant value 48.1 °C is characteristic for PET surface T_g, which is 23.0 °C lower than its bulk T_g determined by DSC. (d) Surface T_g obtained by force-distance curve for PEN films of each thickness. A constant value 85.4 °C is characteristic for PEN surface T_g, which is 26.6 °C lower than its bulk T_g determined by DSC. Only 9 nm thick film showed a different surface T_g at 89.8 °C. [Color figure can be viewed at wileyonlinelibrary.com.]

significantly slowed as polymer films become very thin,[34] and a dielectric spectroscopy study that showed the reduction in chain mobility at the very interface with substrate significantly slowing crystallization processes in polyhydroxybutyrate (PHB).[35]

Measurement of the surface T_g can give a better understanding of the surface crystallization phenomenon. In this study, SFM force-distance curve measurement was used to determine the surface T_g of PET and PEN films, which can detect the slight change in elasticity on the surface.[26,27]

Figure 8(a,b) are typical examples of T_g determination by force-distance curve measurement for PET and PEN, respectively. There is an obvious change in slope at temperatures associated with the surface T_g. Likewise, surface T_g for other thicknesses were determined and shown in Figure 8(c) for PET and Figure 8(d) for PEN. From these force-distance curve experiments a surface T_g for PET (48.1 °C) and PEN (85.4 °C) were exhibited, regardless of the film thickness. The surface T_g of PET and PEN are 23.0 and 26.6 °C, respectively, below their bulk T_g obtained by DSC. The surface T_c of PET (Figure 1) and PEN (Figure 4) are also confirmed to be much smaller than their bulk T_c, which is consistent with the infrared spectroscopic study on PET.[36]

The thermal transition temperatures observed in PET and PEN films are summarized in Table I. As this table shows, in all cases the crystallization process onsets at some temperature greater than the T_g, as has been widely observed elsewhere, and this T_c-T_g for cold crystallization of the PEN bulk is greater than for the PET bulk as shown, for example in,[37] likely a result of the lower chain flexibility of the PEN molecule, to allow ordering during crystallization.

In both polymers, the difference between the T_c and the T_g is greater at the surface than in the bulk, reflecting the more confined environment for crystallization leading to a greater T_c-T_g required for crystallization to start, in a similar way to the increased temperature for the onset of crystallization observed here in the very thinnest films. The effect of the greater stiffness of the PEN molecular structure compared with PET becomes even more pronounced in the near-surface region where there is more chain confinement within the narrow mobile near-surface region, meaning that the T_c-T_g approaches 30 °C.

The lower surface T_g is explained by the greater chain mobility close to the film surface, which influences dynamic parameters of polymer chains.[38–41] According to this notion, some length scale exists which increases as the temperature decreases, meaning

Table I. Thermal Events of PET and PEN

| Events | Analysis | Temperature (°C) | | Temperature difference (°C) |
		PET	PEN	PEN-PET
Surface T_g	FD curve	48.1	85.4	37.3
Surface T_c	AFM	70	115	45
Surf. $T_c - T_g$		22	30	8
Bulk T_g	DSC	71.1	112	40.9
Bulk T_c	AFM	>85[a]	>130[b]	45
Bulk $T_c - T_g$		14	18	4

[a] Increases as thickness becomes less than 70 nm.
[b] Increases as thickness becomes less than 60 nm.

that larger parts need to move cooperatively to commence any thermal activity. Keddie *et al.*[17] estimated the characteristic length scale of PS, as 8.0 ± 0.8 nm from the calculation by additive law between the expansivity of the surface and bulk layers. A study on the surface dynamics of PS films probed by muons[42] clarified that there is a dynamically distinct surface layer, of ca. 10–25 nm thickness at 20–30 °C below bulk T_g, near the surface, which enlarges rapidly to infinity as the temperature reaches to bulk T_g. The thickness of the PET surface layer was determined from SFM force-distance curve measurements of T_g[27] to be 13.6 nm irrespective of overall film thickness. When the surface layer is capped with a thin gold layer, it was reported that the surface-enhanced molecular mobility was supressed,[23] implying the direct exposure of the surface molecules to the air is important for the higher mobility of the molecules and depressed T_g and T_c.

In this study, it was demonstrated that both the surface T_g and the surface T_c (the first observation of crystals at the surface) are constant in both PET and PEN films with various thicknesses (Figures 1, 4, and 8), even though films of different thickness exhibit different molecular anisotropy and a range of crystal growth rates. Thus these thermal transitions are thought to be led by the molecules within the surface region (the depth of the surface region being independent of film thickness) which are those of the highest mobility. In the case of surface T_c, the key step is the sporadic generation of nascent crystal cores on the surface, which can protrude into free space making them free from the confinement of anisotropic chain orientation in thin films. On the other hand, the subsequent crystal growth, the rate of which is thickness dependant, needs to reel-in numerous molecules in the surface layer, influenced by the
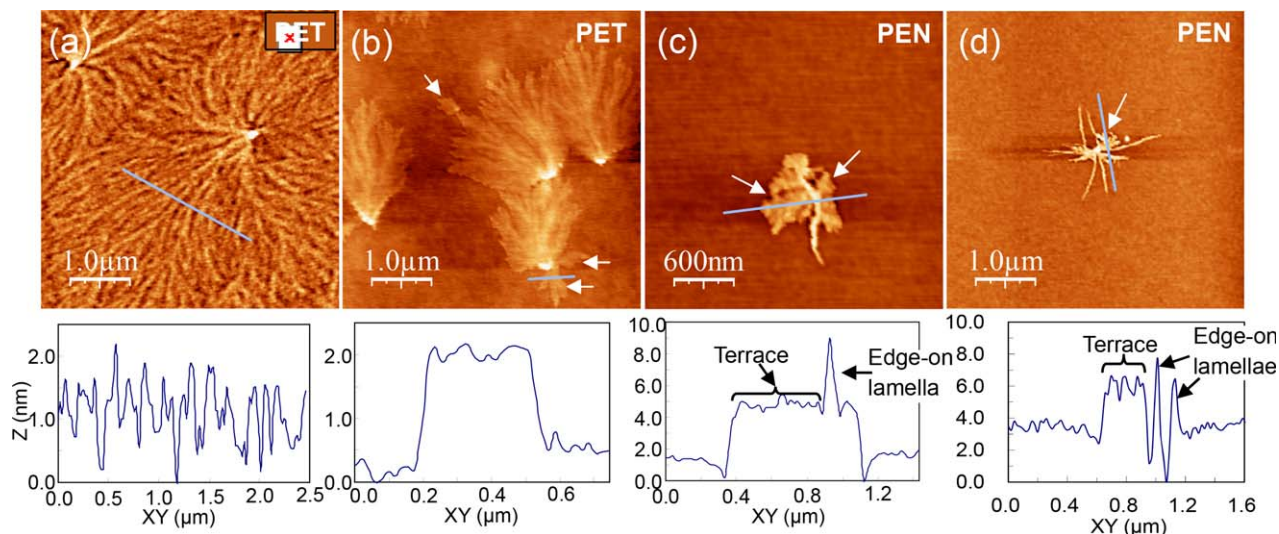

Figure 9. (a) PET surface crystals (film thickness 39.3 nm, annealed at 85 °C) shows ridge-like morphology, which consists of numerous stacked edge-on lamellar crystals. The height profile (below) indicates the individual, narrow, nature of the lamellae. (b) Terraces (indicated by arrows) with thickness of around 2 nm appeared on the surface crystals of a 680 nm thick PET film annealed at 75 °C. Their cross section (below) does not show ridge-like shape, rather a plateaued profile to the terraces. (c) A 16 nm thick PEN film annealed at 115 °C produced an S-shaped edge-on crystal, followed by derivative terraces (indicated by arrows) adjacent to it. The height profile (below) indicates the protruding nature of the original S-shaped crystal and the terraced nature of the surrounding crystal. (d) A 9 nm thick film annealed at 125 °C showed several edge-on lamellae but also small terrace-like crystals (indicated by the arrow). The height profile shows the protruding edge-on crystals and a terrace-like crystal at the very beginning stage of development. [Color figure can be viewed at wileyonlinelibrary.com.]

molecular anisotropy due to thickness confinement, the flexibility of the polymer chain, and the influence of the substrate.

The existence of a surface region helps us to better understand the generation of 2D surface crystals which appear below bulk T_c. As the surface T_c is less than bulk T_c, the growth of surface crystals downwards is limited, because the polymer molecules in the bulk layer are still not sufficiently mobile to be crystallized in the temperature range between surface T_c and bulk T_c. Even though it is still not easy to directly measure the thickness of the surface crystals, it is likely determined by the surface layer thickness.

Lamellar Orientation in the PET Surface Crystals

Grazing incidence X-ray, and electron microscopy studies of PET have shown preferential crystallization at the surface with edge-on crystals[13,14,43–45] in some cases with terrace-like flat-on crystals at the growth front of the edge-on lamellae. Short linear aliphatic polyester thin films, poly(propylene succinate) (PPS), poly(propylene glutarate) (PPG), and poly(propylene adipate) (PPA), also showed edge-on lamellar orientation,[46] consistent with a Monte Carlo simulations.[47]

In this study, PET surface crystals showed a ridge-like profile which is associated with edge-on stacked lamellae. The wavelength of the surface crystals exhibits a clear dependence on film thickness, hence the lamellar orientation is thought to be edge-on with quite a well-defined lamellar thickness. The line profile in Figure 9(a) (film thickness 39 nm) exemplifies the edge-on lamellar crystals that are reported in the literature.[13,14,43,44,46] The terraces observed in the early stages of a lamella formation, for example, those marked by arrows in Figure 9(b) (film thickness 680 nm) might correspond to flat-on lamellar crystals.[14,45] The flat-on crystals seem to be a nascent structure of the surface crystals in PET, with the morphological features of diffusion-limited aggregation. The emergence of the flat-on terraces always precedes the growth of edge-on crystals, and as the edge-on lamellae develop, the flat-on crystals are eventually absorbed or integrated into the edge-on crystals.

Thus, the following model could be postulated: As the temperature of a film is raised above surface T_g, molecular mobility with cooperative motion in the surface layer increases; there should be some gradation in the molecular thermal mobility in the surface layer, and the most outward molecules are preferentially crystallized forming flat-on terraces – at this stage there is not enough space to form edge-on lamellae which will grow downwards but only flat-on lamellae with horizontal growth; as crystallization develops, and there is more time for motion deeper into the surface the flat-on growth is taken over by the preferred edge-on lamellae.

Lamellar Orientation in the PEN Surface Crystals

For most thicknesses of PEN, the ridged morphology, similar to that of mature PET crystals, is observed in PEN right from the start of growth, and this is also associated with a full 360° growth angle away from the nucleus right from the start (Supporting Information), in contrast to PET which first forms flat-on terraces over a narrow angular range proceeds at the growth front of fan-shape edge-on crystals (Figures 2 and 9) initially before the 360° growth of ridged lamellae is observed.

The very thin films of PEN [see Figures 9(c,d) and [7](d)] firstly generate highly protruding surface crystal embryos. In Figure 9(c,d) these initial crystals are clearly S- or C-shaped (such morphologies are reminiscent of those previously observed in polyethylene[2,48–52]) In other polymer thin films, for example, poly[L-lactide] (PLLA),[7,9] an S-shape or C-shape edge-on embryo crystal first forms and subsequently flat-on surface crystals branch from the edge-on crystals as its stem. The preferred direction of the curvature of edge-on lamellae has been linked with the chirality of the polyenantiomer,[53,54] or the molecular weight ratio of a polymer blend,[55] however, as expected, the edge-on crystals of (non-chiral) PEN show both left-hand and right-hand directions of curvature here [Figure 5(F2)].

In the case of PEN ultrathin films in this study, lamellae with characteristic habit of terraces emerge from the initial edge-on crystals [Figure 9(c,d)]. The lamellar orientation of the PEN terrace-like crystals, however, is not directly observable from the results in this study. We can only speculate that the terrace-like crystals have flat-on orientation based on their morphological features, that is, their height profiles are relatively flat, and the edges slightly fringed due to diffusion-limited growth.[56,57] Thus, PEN appears to favor an edge-on embryo surface crystal, which, in thicker films, can directly give rise to edge-on lamellae in all directions within the plane. In ultra-thin PEN crystals, however, the growth of ridged lamellae appears constrained (as it was in the low temperature stages of growth for the PET), but the terraced (perhaps "flat-on") crystals can grow to a limited extent from the initial edge-on embryo. The difference between PET and PEN surface crystal development in the early stages can be accounted for by the preference for PEN to form an edge-on initial crystal, and hence, in contrast to PET, the terraced morphology is only observed in the case of the ultrathin films where, even at elevated temperatures, the surface mobility is very highly constrained.

It has been reported that the degree of supercooling and the surface free energy of the substrate both influence the lamellar orientation at the substrate layer.[58] The thermal history is also reported[59] to influence the lamellar orientation: "cast and annealed thin films" give edge-on lamellae, whereas "melt crystallized thin films" develop flat-on lamellae. A numerical simulation study[25] also suggests that cold crystallization gives nascent crystals with predominantly edge-on orientation, as the crystal side-surface has a relatively low free energy at the free surface. Thus, in the current study, in which the films are cast and annealed, the films are cast on a low surface energy substrate, and crystallized at high supercooling, it is consistent with the previous studies that edge-on crystals are the principal means of crystallization.

Lamellar orientation tendency of PET and PEN are summarized in Figure 10. Note that the lamellar orientations here are consistently speculated conclusions based on the morphological features. Further investigations by means of *in situ* electron diffractometry are needed for a better understanding of these crystallization behaviors.
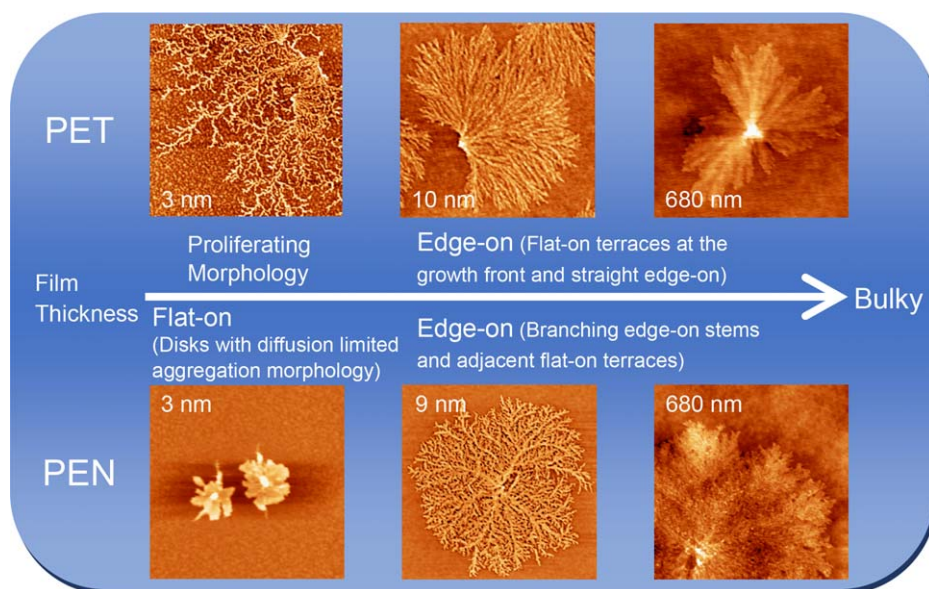
Figure 10. Lamellar orientation behavior of PET and PEN surface crystals. Surface crystals appear even on bulk-like thick films (thickness 680 nm), and edge-on lamellae are clearly observable in the thickness range between about 10–40 nm. In the case of ultrathin films (thickness 3 nm), flat-on disks appear for PEN whereas proliferating surface crystals (lamellar orientation is unknown) develop for PET. [Color figure can be viewed at wileyonlinelibrary.com.]

Difference Between PET and PEN Surface Crystals

In the case of PET the co-linear attachment of ethylene glycol diester residues to the phenyl ring makes the PET chains more flexible than those of the PEN with the longer naphthyl rings without co-linear attachment. The unit cell parameter, c, of PEN is longer than that of PET by more than 23%.[60] As a consequence, bulk T_g and bulk T_c of PET is lower than that of PEN, static conformations such as rms end-to-end distance $<r^2>_0$ is smaller for PET than PEN. The different chain flexibility is reflected in numerous physical properties such as dynamic mechanical properties,[61,62] electric charge relaxation,[63] and gas permeation.[64–66] In this case, the chemical similarity of PET and PEN gives rise to many similar characteristics of surface mobility and surface crystallization, but transition temperatures and the degree to which the confining effect either of the ultrathin films and/or the chain mobility being confined to the very near surface are influenced by the more rigid chains of the PEN.

This greater molecular flexibility of PET is thought to be the reason for the straight-shape morphology of the edge-on lamellae on PET surface crystals. The sufficient molecular flexibility of PET chains enables the higher molecular self-diffusivity which results in the lower thermal transition temperatures and its intrinsic crystal morphology. In the case of PEN crystals, the smaller molecular flexibility and self-diffusivity are thought to induce branching aggregation on the activated sites on the lamella where some advantageous geometry such as a step or kink is available. Due to the rigid structure, PEN molecular chains produce complicated branching morphology of the surface crystals. It is apparently also responsible for the propensity of PEN to form edge-on embryo crystals.

CONCLUSIONS

1. The crystal stability diagrams of PET and PEN were compared. In both cases the surface crystals appeared at surface T_c about 15 °C under the bulk T_c, and were superseded at the bulk T_c by bulk crystals. When the thickness of the film is less than 70 nm (PET) or 60 nm (PEN), significant increases of the bulk T_c were observed; surface crystals were stable at temperatures much higher than the normal bulk T_c. The surface T_c of PET and PEN show a constant value, except for the thinnest 3 nm thick films.

2. Force-distance curve measurements detected significant surface T_g depression of PET and PEN (22.0 and 26.6 °C respectively, irrespective of film thickness), compared with their bulk T_g. These surface T_g depressions imply that the enhanced chain mobility with cooperative motion exists near the surface.

3. The lamellar orientation of PET surface crystals is thought to be stacked edge-on lamellae with flat-on terraces at the growth front. PEN surface crystals are also thought to emerge from embryo edge-on lamellae.

4. The morphological differences of surface crystals such as the straight-shape lamellae for PET, and finely branched lamellae for PEN are attributed to the difference in chain flexibility, and hence molecular motion to the crystal growth front, between PET and PEN.

REFERENCES

1. Bassett, D. C. Principles of Polymer Morphology; Cambridge University Press, Cambridge, UK, **1987**.

2. Vaughan, A. S.; Bassett, D. C. In Comprehensive Polymer Science; Polymer Properties, Pergamon Press, Oxford, UK, **1989**; Vol. *2*.

3. Bassett, D. C.; Olley, R. H. *Polymer* **1984**, *25*, 935.

4. Taguchi, K.; Miyaji, H.; Izumi, K.; Hoshino, A.; Miyamoto, Y.; Kokawa, R. *Polymer* **2001**, *42*, 7443.

5. Taguchi, K.; Miyamoto, Y.; Miyaji, H.; Izumi, K. *Macromolecules* **2003**, *36*, 5208.

6. Taguchi, K.; Miyaji, H.; Izumi, K.; Hoshino, A.; Miyamoto, Y.; Kokawa, R. *J. Macromol. Sci.* **2002**, *B41*, 1033.

7. Kikkawa, Y.; Abe, H.; Iwata, T.; Inoue, Y.; Doi, Y. *Biomacromolecules* **2001**, *2*, 940.

8. Kikkawa, Y.; Abe, H.; Iwata, T.; Inoue, Y.; Doi, Y. *Biomacromolecules* **2002**, *3*, 350.

9. Kikkawa, Y.; Abe, H.; Fujita, M.; Iwata, T.; Inoue, Y.; Doi, Y. *Macromol. Chem. Phys.* **2003**, *204*, 1822.

10. Reiter, G.; Sommer, J. *J. Chem. Phys.* **2000**, *112*, 4376.

11. Reiter, G.; Sommer, J. *J. Chem. Phys.* **2000**, *112*, 4384.

12. Reiter, G. *J. Polym. Sci. B: Polym. Phys.* **2003**, *41*, 1869.

13. Sakai, Y.; Imai, M.; Kaji, K.; Tsuji, M. *J. Cryst. Growth* **1999**, *203*, 244.

14. Sakai, Y.; Imai, M.; Kaji, K.; Tsuji, M. *Macromolecules* **1996**, *29*, 8830.

15. Keddie, J. L.; Jones, R. A. L.; Cory, R. A. *Faraday Discuss.* **1994**, *98*, 219.

16. Forrest, J. A.; Dalnoki-Veress, K.; Stevens, J. R.; Dutcher, J. R. *Phys. Rev. Lett.* **1996**, *77*, 2002.

17. Keddie, J. L.; Jones, R. A. L.; Cory, R. A. *Europhys. Lett.* **1994**, *27*, 59.

18. Forrest, J. A.; Svanberg, C.; Revesz, K.; Rodahl, M.; Torell, L. M.; Kasemo, B. *Phys. Rev. E* **1998**, *58*, R1226.

19. Fryer, D. S.; Nealey, P. F.; de Pablo, J. J. *Macromolecules* **2000**, *33*, 6439.

20. Jean, Y. C.; Zhang, R.; Cao, H.; Yuan, J. P.; Huang, C. M. *Phys. Rev. B* **1997**, *56*, R8459.

21. Morita, H.; Tanaka, K.; Kajiyama, T.; Nishi, T.; Doi, M. *Macromolecules* **2006**, *39*, 6233.

22. Campoy-Quiles, M.; Sims, M.; Etchegoin, P. G.; Bradley, D. D. C. *Macromolecules* **2006**, *39*, 7673.

23. Zhu, L.; Jona, J.; Nagapudi, K.; Wu, T. *Pharm. Res.* **2010**, *27*, 1558.

24. Wu, T.; Yu, L. *Pharm. Res.* **2006**, *23*, 2350.

25. Yamamoto, T. *J. Chem. Phys.* **2013**, *139*, 054903.

26. Bliznyuk, V. N.; Assender, H. E.; Briggs, G. A. D. *Macromolecules* **2002**, *35*, 6613.

27. Shinotsuka, K.; Bliznyuk, V. N.; Assender, H. E. *Polymer* **2012**, *53*, 5554.

28. Despotopoulou, M. M.; Miller, R. D.; Rabolt, J. F.; Frank, C. W. *J. Polym. Sci. B: Polym. Phys.* **1996**, *34*, 2335.

29. Zhokhavets, U.; Gobsch, G.; Hoppe, H.; Sariciftci, N. S. *Thin Solid Films* **2004**, *451*, 69.

30. Cimrova, V.; Neher, D.; Kostromine, S.; Bieringer, T. *Macromolecules* **1999**, *32*, 8496.

31. Wang, Y.; Chan, C. M.; Ng, K. M. *Macromolecules* **2008**, *41*, 2548.

32. Jukes, P. C.; Das, A.; Durell, M.; Trolley, D.; Higgins, A. M.; Geoghegan, M.; Macdonald, J. M.; Jones, R. A. L.; Brown, S.; Thompson, P. *Macromolecules* **2005**, *38*, 2315.

33. Baldenegro-Perez, L. A; Navarro-Rodriguez, D.; Medellin-Rodriguez, F. J.; Hsiao, B.; ; Avila-Orta, C. A.; Sics, I. *Polymers* **2014**, *6*, 583.

34. Tang, Q.; Hu, W.; Napolitano, S. *Phys. Rev. Lett.* **2014**, *112*, 148306.

35. Napolitano, S.; Wübbenhorst, M. *Macromolecules* **2006**, *39*, 5967.

36. Bertoldo, M.; Labardi, M.; Rotella, C.; Capaccioli, S. *Polymer* **2010**, *51*, 3660.

37. Montserrat, S.; Roman, F.; Colomer, P. *J. Therm. Anal. Calorim.* **2003**, *72*, 657.

38. Adam, G.; Gibbs, J. H. *J. Chem. Phys.* **1965**, *43*, 139.

39. Cohen, M. H.; Grest, G. S. *Phys. Rev. B* **1979**, *20*, 1077.

40. Fischer, E. W.; Donth, E.; Steffen, W. *Phys. Rev. Lett.* **1992**, *68*, 2344.

41. Forrest, J. A.; Mattsson, J. *Phys. Rev. E* **2000**, *61*, R53.

42. Pratt, F. L.; Lancaster, T.; Brooks, M. L.; Blundell, S. J.; Prokscha, T.; Morenzoni, E.; Suter, A.; Luetkens, H.; Khasanov, R.; Shinotsuka, K.; Assender, H. E. *Phys. Rev. B* **2005**, *72*, 121401R-1-4.

43. Durell, M.; Macdonald, J. E.; Trolley, D.; Wehrum, A.; Jukes, P. C.; Jones, R. A. L.; Walker, C. J.; Brown, S. *Europhys. Lett.* **2002**, *58*, 844.

44. Macdonald, J. E.; Durell, M.; Trolley, D.; Lei, C.; Das, A.; Jukes, P. C.; Geoghegan, M.; Higgins, A. M.; Jones, R. A. L. *Radiat. Phys. Chem.* **2004**, *71*, 811.

45. Haubruge, H. G.; Daussin, R.; Jonas, A. M.; Legras, R. *Polymer* **2003**, *44*, 8053.

46. Hernandez, J. J.; Rueda, D. R.; Garcia-Gutierrez, M. C.; Nogales, A.; Ezquerra, T. A.; Soccio, M.; Lotti, N.; Munari, A. *Langmuir* **2010**, *26*, 10731.

47. Ma, Y.; Hu, W. B.; Reiter, G. *Macromolecules* **2006**, *39*, 5159.

48. Bassett, D. C.; Hodge, A. M. *Polymer* **1978**, *19*, 469.

49. Bassett, D. C. *J. Macromol. Sci.* **2003**, *B42*, 227.

50. Patel, D.; Bassett, D. C. *Polymer* **2002**, *43*, 3795.

51. Keith, H. D.; Padden Jr., F. J. *J. Appl. Phys.* **1963**, *34*, 2409.

52. Keith, H. D.; Padden Jr., F. J. *Polymer* **1984**, *25*, 28.

53. Maillard, D.; Prud'homme, R. E. *Macromolecules* **2008**, *41*, 1705.

54. Wang, X.; Prud'homme, R. E. *Macromolecules* **2014**, *47*, 668.

55. Marubayashi, H.; Nobuoka, T.; Iwamoto, S.; Takemura, A.; Iwata, T. *ACS Macro Lett.* **2013**, *2*, 355.

56. Yang, P.; Han, Y. *Langmuir* **2009**, *25*, 9960.

57. Lin, D.-W.; Zhong, Z.; Tang, Y.-R.; Gao, Y.; He, Y.-N.; Guo, B.-H.; Xu, J. *Chin. J. Polym. Sci.* **2014**, 1234.

58. Yang, J. P.; Liao, Q.; Zhou, J. J.; Jiang, X.; Wang, X. H.; Zhang, Y.; Jiang, S. D.; Yan, S. K.; Li, L. *Macromolecules* **2011**, *44*, 3511.

59. Lee, J. S.; Prabu, A. A.; Kim, K. J. *Polymer* **2010**, *51*, 6319.

60. Tonelli, A. E. *Polymer* **2002**, *43*, 637.

61. van den Heuvel, C. J. M.; Klop, E. A. *Polymer* **2000**, *41*, 4249.

62. Aoki, Y.; Li, L.; Amari, T.; Nishimura, K.; Arashiro, Y. *Macromolecules* **1999**, *32*, 1923.

63. Canadas, J. C.; Diego, J. A.; Sellares, J.; Mudarra, M.; Belana, J. *Polymer* **2000**, *41*, 8393.

64. McDowell, C. C.; Freeman, B. D.; McNeely, G. W.; Haider, M. I.; Hill, A. J. *J. Polym. Sci. B: Polym. Phys.* **1998**, *36*, 2981.

65. McGonigle, E. A.; Liggat, J. J.; Pethrick, R. A.; Jenkins, S. D.; Daly, J. H.; Hayward, D. *Polymer* **2001**, *42*, 2413.

66. Pavel, D.; Shanks, R. *Polymer* **2003**, *44*, 6713.